Materials Science and Engineering A 513–514 (2009) 1–7

Contents lists available at ScienceDirect

Materials Science and Engineering A

journal homepage: www.elsevier.com/locate/msea

Dynamic strain aging effects on low-cycle fatigue of AISI 430F

M. Avalos*, I. Alvarez-Armas, A.F. Armas

Instituto de Física de Rosario, CONICET - Universidad Nacional de Rosario, 27de Febrero 210 bis, Rosario 2000, Argentina

ARTICLE INFO

Article history:
Received 26 July 2008
Received in revised form
28 November 2008
Accepted 16 January 2009

Keywords:
Low-cycle fatigue
Cyclic hardening
Stainless steels
Dynamic strain aging

ABSTRACT

The effects of dynamic strain aging (DSA) on the cyclic mechanical behavior were investigated in a ferritic steel type AISI 430F. Strain-rate changes performed during cyclic tests show a negative strain-rate dependence of the flow stress for temperatures ranging from 200 °C to 450 °C. Low-cycle fatigue curves exhibit prominent cyclic hardening at 400 °C and 450 °C. The influence of the embrittlement phenomena on the hardening of this ferritic steel was also investigated by performing aging treatments at 400 °C and 450 °C in the alloy. These results suggest that a DSA mechanism is operative in this material in a temperature range between 300 °C and 400 °C. Stress relaxation experimental results are also discussed in terms of dynamic strain aging.

© 2009 Published by Elsevier B.V.

1. Introduction

The term dynamic strain aging (DSA), denotes a process of aging that takes place during plastic deformation. Over a particular strain rate and temperature range, the interactions between solute atoms and dislocations result in a strong pinning of dislocations, responsible for strain aging. Higher stress levels are required to produce further straining of the material, either to pull dislocations free from the pinning atoms or to nucleate fresh dislocations. Thus, the main effects of dynamic strain aging on the mechanical properties of materials during cyclic tests are an inverse dependence of the peak tensile stress on strain rate, an unusual increase in cyclic hardening and a serrated flow known as the Portevin-Le Chatelier (PLC) effect [1,2]. The appearance of serrations provides useful information to evaluate the kind of atoms that interact with dislocations to cause the DSA. Different authors [3,4] have concluded that serrations appear over a narrower range of temperatures and strain rates than what is necessary for the development of DSA. In this investigation it was proposed to perform stress relaxation tests (SRT) as an alternative approach for investigating which elements might be responsible for dynamic strain aging. In stress relaxation tests, the crosshead motion of the testing machine is suddenly stopped during the tensile or compression part of the fatigue hysteresis loop at a desired strain, and the stress is allowed to relax over a period of time. The stress decreases with time, and a relaxation curve is obtained. From the study of the SRT curves, it is possible to estimate parameters characterizing thermally activated processes. Since the plastic strain due to stress relaxation is negligible, the stress relaxation curves are usually analyzed by assuming the constancy of mobile dislocations ρ and internal stress σ_i. For these experiments it was also assumed that the modulus E is the combined elastic modulus of the testing system including the specimen. Considering that DSA is a phenomenon that affects deformation dynamics, it is reasonable to assume that it affects the dynamics of SRT curves as well as the low-cycle fatigue response.

Low-cycle fatigue constitutes a technological problem in structural parts or industrial equipment and it is particularly important at intermediate temperatures. The temperature dependence of low-cycle fatigue is an important aspect for material exposed to service above room temperature. If the regime of temperatures lies in the DSA temperature range, the influence of DSA on the mechanical behavior of the alloy becomes an important matter, as well. In the case of stainless steels, extensive studies on cyclic properties at temperatures up to 600 °C (intermediate temperatures) are available in the literature. Most of these investigations concentrate on austenitic alloys [4–8], and only a few deal with ferritic stainless steels [9]. The different results strongly suggest that both DSA and environmental effects should be considered when analyzing the evolution of the cyclic stress–strain response and fatigue life at a given temperature. In particular, in this study we concentrate on the ferritic stainless steel AISI 430F.

High-stress corrosion resistance and relatively lower production costs are the main reasons for increased applications of AISI 430F. It is one of the most widely used commercial intermediate-chromium ferritic alloys, and is found in automotive, chemical and food-processing applications. This alloy combines a suitable corrosion

* Corresponding author. Tel.: +54 341 485 3200; fax: +54 341 482 1772.
E-mail address: avalos@ifir-conicet.gov.ar (M. Avalos).

0921-5093/$ – see front matter © 2009 Published by Elsevier B.V.
doi:10.1016/j.msea.2009.01.047

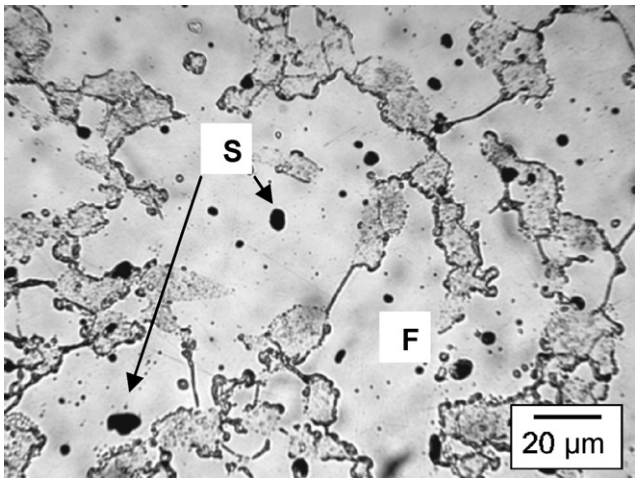

Fig. 1. Optical micrograph of sample HT. The microstructure consist of a ferritic matrix, F, which contains sulfide inclusions, S.

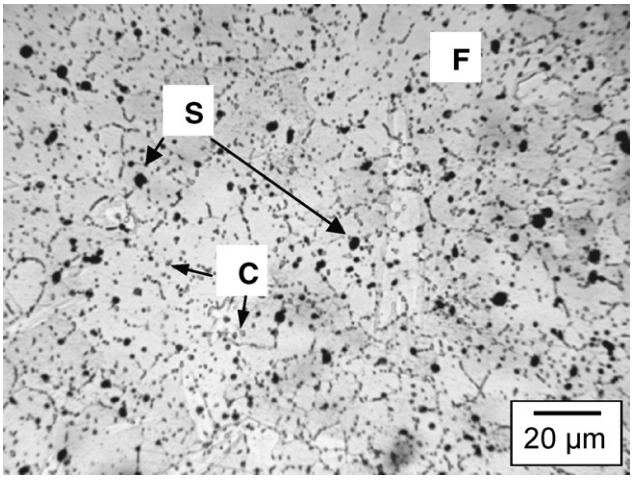

Fig. 2. Optical micrograph of sample AT. The microstructure consist of a ferritic matrix, F, carbides, C, and sulfide inclusions, S.

and oxidation resistance with the advantage of being easy cold worked. However, problems such as low ductility, and loss of fracture toughness when exposed to intermediate temperatures are present in this steel. Our objective was to explore nonconventional properties that the material exhibits in order to offer alternatives choices for potential applications in engineering design. In particular, in AISI 430F, the cyclic stress–strain behaviors that occur in the dynamic strain aging regime have not yet been clearly identified and further investigation of the fatigue deformation accompanying dynamic strain aging is needed.

The aim of this work is to study the influence of the DSA on the cyclic behavior of AISI 430F. During low-cycle fatigue tests, strain-rate and test-temperature changes were made to investigate the effect of DSA on fatigue behavior. We also analyzed the dynamic strain aging effects through the stress relaxation tests.

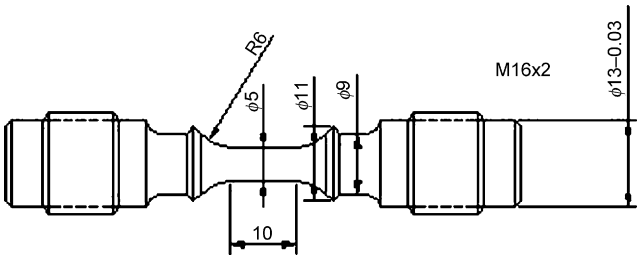

Fig. 3. Low-cycle fatigue test specimen.

2. Experimental procedure

The material used in this study was type AISI 430F ferritic steel supplied in the form of 19 mm diameter cylindrical bars. The alloy had a chemical composition of (in wt.%): 0.11 C; 0.34 Si; 1.0 Mn; 0.023 P; 0.3 S; 17.0 Cr; and 0.23 Mo. P and S are added to improve the machinability of the material. Two different heat treatments were applied to the specimens: a high temperature treatment at 1000 °C for 2 h followed by air cooling and a lower temperature annealing treatment of 750 °C for 3 h, also followed by air cooling. We will denote the high temperature and annealing treatments as HT and AT, respectively. The microstructure of the HT samples consists of a volume fraction of 20% of martensitic contained in a ferritic matrix (F) which is free of carbides but contains sulfide inclusions (S) (Fig. 1). The grain size is about 30 μm. In contrast, the microstructure of the AT samples is homogeneous ferritic matrix (F) with carbides (C) and sulfide inclusions (S) (Fig. 2). The presence of carbides in the ferritic matrix of the AT samples indicates that there is less carbon and chromium in solid solution in this material's matrix than remains in the HT matrix. For each condition, the microstructure and hardness are listed in Table 1.

Cylindrical specimens for LCF experiments, machined from cylindrical bars, had a gage length and diameter of 10 mm and 5 mm, respectively (Fig. 3). Isothermal low-cycle fatigue tests were carried out under fully reversed total-strain control, applying a triangular waveform at a constant total strain rate of $\dot{\varepsilon} = 1 \times 10^{-3}\, s^{-1}$ over a total-strain range of $\Delta\varepsilon_t = 0.6\%$. The tests were performed in air for temperatures between 20 °C and 500 °C.

The strain-rate sensitivity at different temperatures was analyzed by changing the strain rate over two orders of magnitude during the cyclic tests. Stress relaxation behaviors were analyzed at specific temperatures and a fixed strain of $\varepsilon_t = 0.4\%$ for a relaxation time of 600 s.

Metallographic samples for hardness and microscopy were prepared by grinding and polishing followed by etching with a mixture of 400 ml ethanol, 50 ml HCl, 50 ml HNO_3 and 6 g picric acid. The microstructure was examined by using an optical microscope (OM) and scanning electron microscope (SEM). Extraction replicas were prepared according to a conventional procedure [10]. Replicas were removed from metallographic samples with 10% HCl in methanol and examined in a transmission electron microscopy (TEM) operated at 100 kV. Microhardness testing was performed with a Vickers microhardness tester using loads of 250 g and 500 g. Twenty measurements were performed to evaluate an average value and standard deviation of the parameters.

Table 1
Heat treatment, microstructure and hardness of HT and AT samples of AISI 430F.

Samples	Thermal treatment	Microstructure	Hardness
HT	1000 °C for 2 h. Air cooled	80% ferrite + 20% martensite	200 HV ferrite, 450 HV martensite
AT	Annealing at 750 °C for 3 h. Air cooled	Ferritic matrix with carbides	200 HV

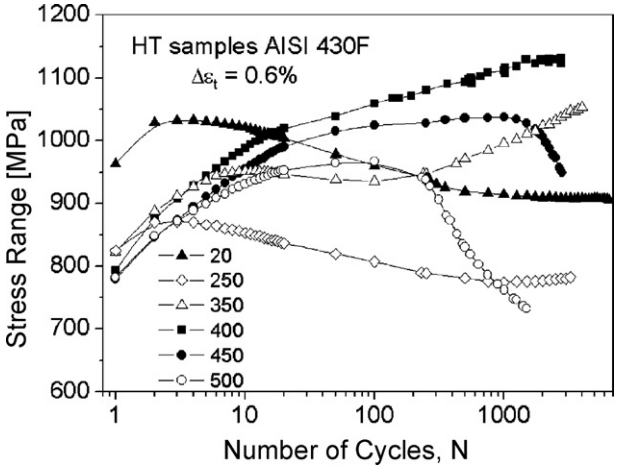

Fig. 4. Stress-range evolution during LCF tests at different temperatures performed on HT samples of AISI 430F.

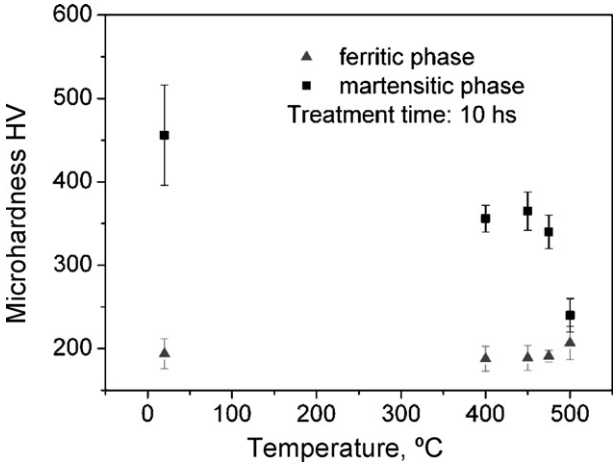

Fig. 6. Microhardness of the ferritic and martensitic phases in HT samples of AISI 430F taken after different temperature treatments.

3. Results and discussion

3.1. Cyclic deformation test

The cyclic hardening-softening curves of AISI 430F are shown in Fig. 4, for temperatures between 20 °C and 500 °C, $\dot{\varepsilon} = 1 \times 10^{-3}\, s^{-1}$ and $\Delta\varepsilon_t = 6.0 \times 10^{-3}$. In this figure the resulting stress range is plotted against the number of cycles. It is evident that the cyclic response is strongly temperature-dependent. All the curves display a comparable initial hardening of almost 10% between cycles one and two. In this work it was assumed that the peak tensile stress of the first cycle ($N = 1$) is representative of a monotonic tensile stress, as there was no previous cyclic reversion. For each curve, this monotonic stress decreases from room temperature up to 250 °C where it becomes nearly temperature independent up to 500 °C. This anomalous behavior will be analyzed in a subsequent paragraph together with Fig. 5. Because there were no deformation reversals before the first cycle, we will consider the cyclic behavior as beginning with cycle number two.

At 20 °C, the cyclic tensile stress remains constant for a short number of cycles, followed by a smooth softening that ends in a saturation stage and finally failure. At 250 °C the magnitude of the stress amplitude has decreased, but the cyclic behavior is comparable to that at 20 °C. In contrast, at 350 °C the cyclic behavior is completely different. After an initial hardening, there is a transitional saturation stage, which ends in a linear hardening. At 400 °C the initial hardening region period is more noticeable and it is followed by a secondary hardening stage that continues until rupture. Different authors have reported similar prominent cyclic-hardening behavior in fatigue curves of perlitic [1] and duplex steels [11] and considered it to be a DSA manifestation. The cyclic behavior observed at 450 °C is different from that at 400 °C. Although both curves show an equivalent initial hardening behavior, at 450 °C the secondary hardening is less pronounced and it is followed by a softening up to the failure of the sample. At 500 °C, after the initial hardening and a short stabilization period, a pronounced cyclic softening similar to that of 450 °C occurs. It should be noted that the marked softening reported at 450 °C and 500 °C takes place in an early period of fatigue life with increasing temperatures.

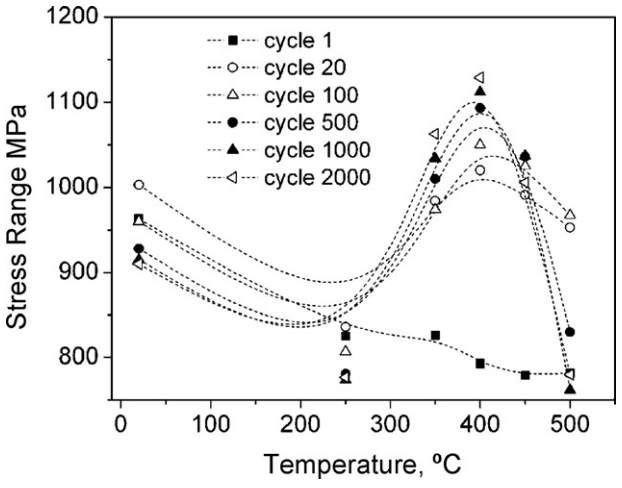

Fig. 5. Stress range as a function of temperature for selected cycles on HT samples of AISI 430F.

To provide a more detailed analysis of the cyclic behavior of this steel, the dependence of the stress range with temperature for selected fatigue cycles is plotted in Fig. 5. As already noted, the flow stress corresponding to the first tensile loading of each curve decreases from room temperature up to 250 °C at which point it becomes nearly temperature independent until 500 °C. Since the peak tensile stress of the first cycle ($N = 1$) is equivalent to a monotonic tensile stress, this dependence of the stress with test temperature can be correlated to the typical aspects of static strain aging reported in tensile tests—an anomalous dependence of flow stress with temperature. Furthermore, it is worth noting that subsequent cycles also show noticeable hardening in the same range of temperature, 250–500 °C. The increment in peak tensile stress is more pronounced between cycles 1000 and 2000 and is maximum at 400 °C.

It is well known that in Fe–Cr alloys exposed to temperatures between 250 °C and 500 °C the ferrite phase can decompose to an iron-rich bcc phase (α) and a chromium-rich bcc phase (α'). This phenomena, known as "475 °C embrittlement", reduces the ductility and toughness of the material and is accompanied by higher mechanical strength and hardness [13]. Since the cyclic hardening of AISI 430F reported in Fig. 4 and the embrittlement can take place over the same temperature range, we were able to study in this investigation the potential influence of the embrittlement phenomena on the hardening on AISI 430F. Aging treatments were performed at the corresponding temperatures for the time durations experienced by the HT samples in the cyclic tests. Fig. 6 shows the evolution of the microhardness of AISI 430F with temperature for aging treatments lasting 10 h. The data indicates that for a time frame equivalent to the period of the test, the aging temperature

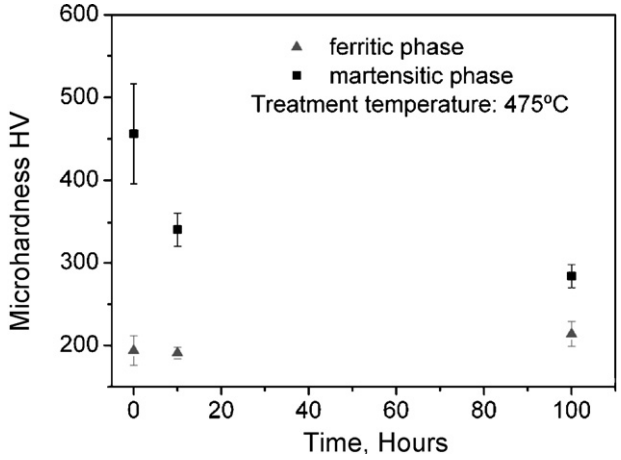

Fig. 7. Microhardness of of the ferritic and martensitic phases in HT samples of AISI 430F after thermal treatment at 475 °C for different times.

does not influence the hardness of the ferritic phase. In the same figure, a decrease in the hardness of the martensitic phase is observed as the temperature increases. According to Speich [12], this effect can be related to changes in the distribution of carbon atoms and the type of structure associated with tempering.

Different authors [13] have shown that an increase in an alloy's chromium content reduces the exposure time at 475 °C required for an increase in hardness and embrittlement. A 40% hardness increase was observed in a 20.6% Cr alloy after a 10 h heat treatment, but no change was seen after a thermal treatment for a similar time in a steel containing 15% of Cr. As shown by our results in Fig. 7, exposures for 100 h at 475 °C result in an increase of about 10% in the hardness of the ferritic phase, while the martensitic phase exhibits decreasing values of hardness with increasing aging times. Therefore, we can conclude that the prominent cyclic hardening shown by our data at 400 °C in AISI 430F cannot be caused by embrittlement due to thermal treatment.

An increase in stress with decreasing strain-rate due to dynamic strain aging has been reported [8,14] in low-cycle fatigue investigations on ferritic and austenitic stainless steels. This inverse strain-rate dependence is important evidence for DSA. In order to analyze the strain-rate influence on the peak tensile stress of hysteresis loops in AISI 430F, strain-rate changes over two orders of magnitude were performed during cyclic tests at different temperatures. Defining $\Delta\sigma_I = \sigma_2 - \sigma_1$ as the difference between the stress range at $\dot{\varepsilon}_1 = 1.0 \times 10^{-3}\,s^{-1}$ and $\dot{\varepsilon}_2 = 1.0 \times 10^{-4}\,s^{-1}$, and $\Delta\sigma_{II} = \sigma_3 - \sigma_2$ as the corresponding difference for $\dot{\varepsilon}_2 = 1.0 \times 10^{-4}\,s^{-1}$ and $\dot{\varepsilon}_3 = 1.0 \times 10^{-5}\,s^{-1}$, negative values of $\Delta\sigma_I$ and $\Delta\sigma_{II}$ correspond to normal behavior for lower peak tensile stress at lower strain rates. Fig. 8(a) and (b) shows these stress differences for various temperatures in HT and AT samples, respectively. In both samples, the stresses exhibit an abnormal behavior between 200 °C and 450 °C with a higher peak tensile stress at lower strain rates. It is well known that such a negative strain rate dependence of the flow stress is a pre-requisite for the PLC effect [3]. However, we must point out that we did not observe the PLC effect in samples tested between 200 °C and 450 °C.

In general, the different mechanisms proposed to explain DSA are related to the interaction between solute atoms and gliding dislocations. Moreover, some of the effects of DSA are likely to be related to the concentration of solute atoms. In particular, in this work we analyze the connection between solute-atom concentration and the prominent cyclic hardening observed in HT samples.

The results presented in Fig. 8(a) and (b) indicate the occurrence of DSA over the temperature range of 200–450 °C in both HT and AT samples of AISI 430F. Considering that the main difference between

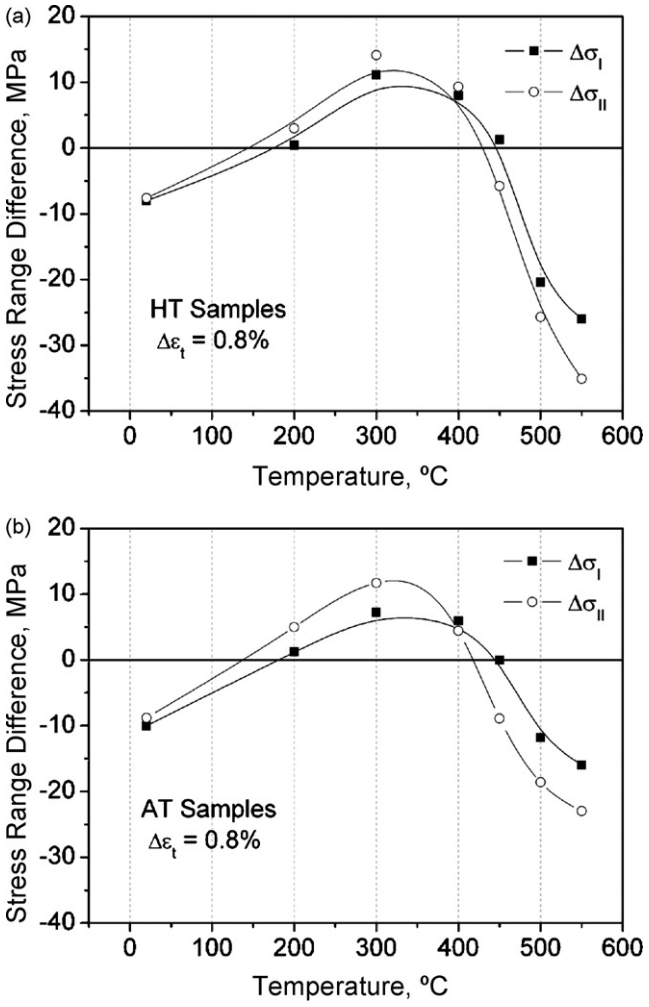

Fig. 8. (a) Stress range difference vs. temperatures for HT samples of AISI 430F. For details see the text. (b) Stress range difference vs. temperatures for AT samples of AISI 430F. For details see the text.

HT and AT samples is the percentage of solute atoms dissolved in the matrix as a solid solution, comparable tests were performed at 400 °C and $\Delta\varepsilon_t = 0.6\%$ using HT and AT samples in order to determine the influence of the concentration of carbon atoms dissolved in the ferritic matrix on the mechanical response (Fig. 9). From the

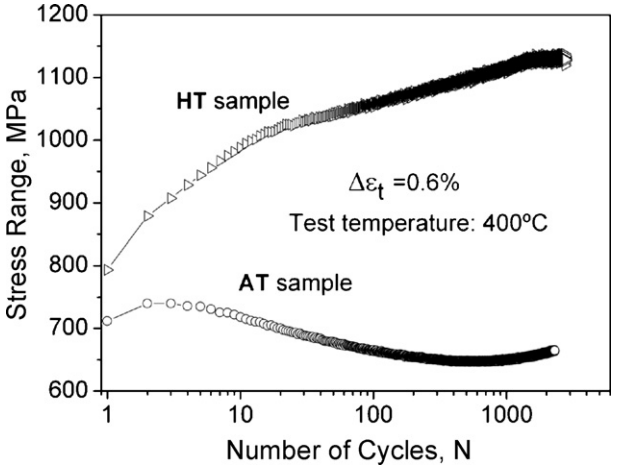

Fig. 9. Cyclic response of AISI 430F with different microstructure corresponding to HT samples and AT samples but cycled at the same thermo-mechanical condition.

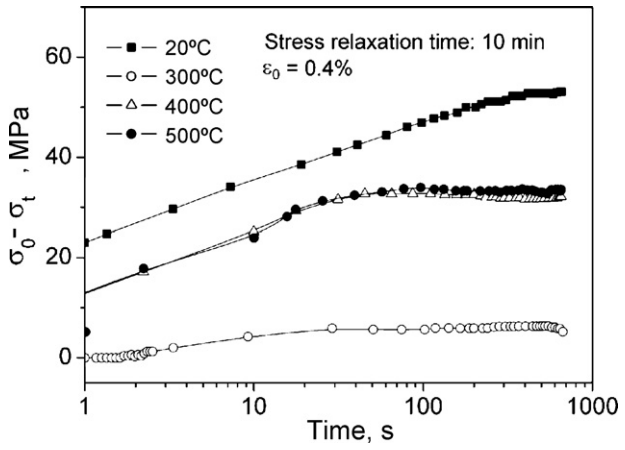

Fig. 10. Evolution of the relaxed stress in HT samples of AISI 430F tested at $\varepsilon_0 = 0.4\%$ and temperatures between 20 °C and 500 °C.

cyclic response of HT and AT samples illustrated in Fig. 9, it is evident that the pronounced hardening effect seen in the HT sample at 400 °C is not observed in the AT sample. The stress amplitude exhibited by AT sample decreases continuously from the beginning of the fatigue process. This result might be rationalized based on the low percentage of solute atoms dissolved in the AT sample's matrix. The hardening effect observed in the HT sample when DSA is active is related to the higher stress levels required to free dislocations from pinning atoms or to nucleate additional dislocations. In contrast, the softening behavior observed in the AT samples, within the temperature range where DSA occurs, indicates that plastic deformation takes place by annihilation and reorganization of mobile dislocations. This finding emphasizes the existence of non-locked dislocations, which can glide to accommodate straining in the AT samples. Hence, the percentage of solute atoms dissolved in solid solution might be a decisive factor for cyclic hardening in the temperature range that corresponds to DSA.

3.2. Stress relaxation behaviors

Stress relaxation experiments are very useful since they provide information about the microscopic mechanisms that control the mobility of the dislocations. Because DSA is a phenomenon that affects dislocation mobility, its occurrence influences such tests. From the analysis of the relaxation curves we propose to estimate a value of a diffusion coefficient and correlate this value with the atoms related to DSA.

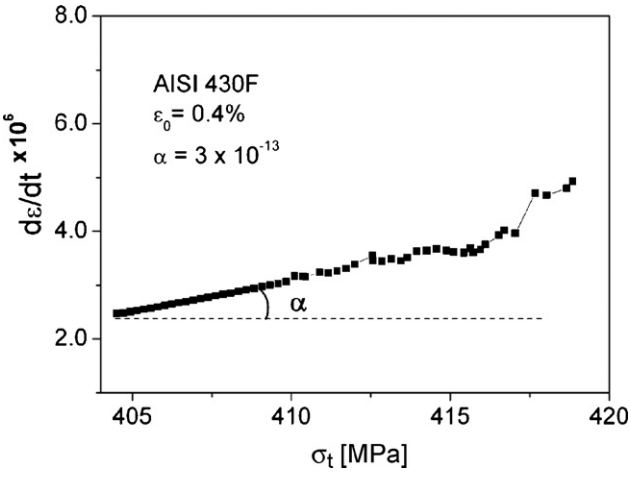

Fig. 11. Strain-rate dependence of the instantaneous stress calculated from the test at 400 °C.

During the stress-relaxation experiments, the specimen is deformed to a total strain ε_0, and the crosshead motion is stopped at time $t = t_0$. The stress, σ_0, is allowed to relax with time. The relaxation curve can then be plotted using either the instantaneous stress σ_t or the relaxed stress, which is the initial stress σ_0 minus the instantaneous stress σ_t. Fig. 10 shows the evolution of the relaxed stress for samples of AISI 430F deformed to $\varepsilon_0 = 0.4\%$ and temperatures between 20 °C and 500 °C. In these tests, we allowed the stress to relax over 10 min. The stress values are accurate within an error of 1%. At room temperature, the value of the relaxed stress continuously increases during the entire hold period. At 300 °C the relaxed stress attains its minimum value, about 10 MPa, and it remains nearly constant throughout the hold. Finally, at higher test temperatures, 400 °C and 500 °C, the relaxed stress first increases for 30 s and then remains constant during the remainder of the test.

The inverse strain-rate dependence of the peak tensile stress for both thermal conditions (Fig. 8(a) and (b)), gives clear evidence of DSA activation between 200 °C and 400 °C, with a maximum effect at 300 °C. The temperature of 300 °C coincides with the temperature of the minimum relaxed stress value observed in Fig. 10. Based on this result, we propose that the behavior of the relaxed stress may be associated with the DSA phenomenon and that the responsible atomic elements can be determined through the instantaneous stress, σ_t.

Taking into account short and long-range obstacles to dislocation motion, the applied stress, σ_a, can be divided into two components:

$$\sigma_a = \sigma_{eff} + \sigma_i \tag{1}$$

where σ_i is the athermal, long-range component of the stress (internal stress) and σ_{eff} is the temperature-dependent, short-range stress component (effective stress). During the stress relaxation process, the effective stress decreases with time and approaches zero as the applied stress tends towards the internal stress, σ_i. In this approach, the internal stress, the mobile dislocation density, ρ and the plastic strain are assumed to remain constant [15].

For materials affected by DSA processes, the applied stress, σ'_a, can be considered to be the sum of the basic stress expected in the absence of a solute strengthening due to DSA, σ_a, and σ_D, which is the contribution of DSA [16]:

$$\sigma'_a = \sigma_a + \sigma_D \tag{2}$$

Combining Eqs. (1) and (2), the applied stress could be written as

$$\sigma'_a = \sigma_{eff} + \sigma_i + \sigma_D \tag{3}$$

During the stress relaxation process in the DSA temperature domain, the effective stress decreases with time, and the applied stress tends to $\sigma_i + \sigma_D$. In this domain, the mechanism associated with DSA, a strong solute–dislocation interaction, can add an extra stress that might not be present in other temperature strain-rate regimens. Thus, it is reasonable to expect a minimum in the relaxed stress at the temperature where the solute and dislocation interactions are strongest. This is in agreement with the curve in Fig. 10.

In the stress relaxation tests, the total strain, made up of the elastic (ε_e) and plastic (ε_p) strain components as $\varepsilon_t = \varepsilon_e + \varepsilon_p$, remains constant and the plastic strain rate can be expressed as [17]

$$\dot{\varepsilon}_p = -\frac{1}{E}\frac{d\sigma_t}{dt} \tag{4}$$

where σ_t is the instant stress, E the young's modulus and t is the time.

When solute atmospheres are formed around dislocations, the rate of dislocation movement and the corresponding strain rate

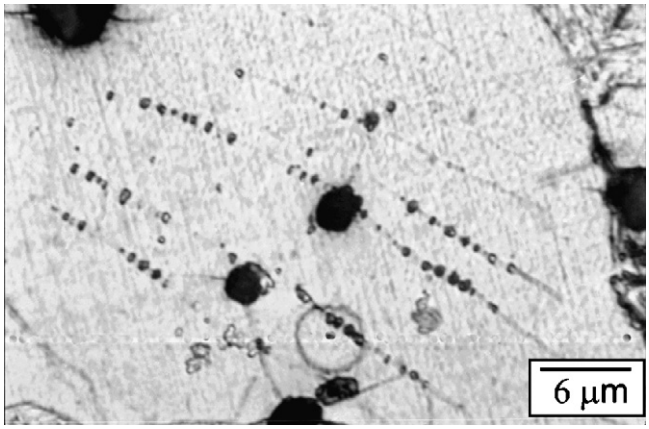

Fig. 12. Optical micrograph of HT sample of AISI 430F cycled over a total strain range $\Delta\varepsilon_t = 0.6\%$ and 400 °C.

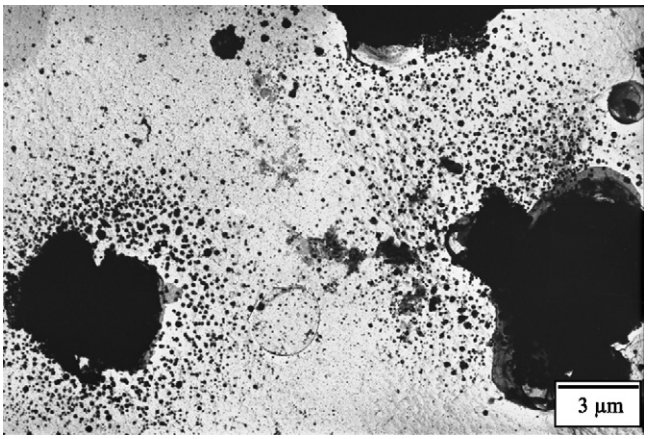

Fig. 14. Extraction replica from an HT sample tested at 500 °C. The TEM observation shows intense carbide growth.

are controlled by the migration velocity of the solute atoms comprising the atmospheres. Therefore, the strain rate of a specimen during a stress-relaxation test should be proportional to the diffusion rate of the solute atoms. Reed Hill and Abbaschian [18] suggest that dislocation movement and the strain rate calculated from a stress-relaxation test should be

$$\dot{\varepsilon} \approx \sigma D \tag{5}$$

where σ is the applied normal stress and D is the diffusion coefficient for the solute atoms associated with DSA.

Eq. (5) can be used to evaluate the diffusion coefficient, D, and to infer which solute atoms are associated with DSA. Fig. 11 shows the strain-rate dependence of the instantaneous stress calculated from the test at 300 °C. The slope of the curve is about 3×10^{-13} in appropriate units. This value is on the order of the diffusion coefficient of carbon atoms at 300 °C as calculated from data in Van Vlack [19]. Based on this result, we conclude that the aging process in AISI 430F is associated with dislocation locking by diffusion of carbon atoms.

3.3. Microstructural evolution

Fig. 12 illustrates the typical microstructure of AISI 430F cycled over a total strain range $\Delta\varepsilon_t = 0.6\%$ at temperatures of 400 °C and 450 °C. The microstructure of the alloy cycled over the same strain range but at 500 °C is shown in Fig. 13. Over temperatures between 250 °C and 500 °C it was observed the development of slip lines in the ferritic matrix, of the type shown in Figs. 12 and 13. The temperature domain in which slip lines are present coincides with those temperatures where DSA is observed, also. This is in fact, a logical coincidence because dynamic strain aging during fatigue increases the tendency of cyclic plastic strain to concentrate in slip bands [20]. At 500 °C (Fig. 13) the slip lines look rather wavy because the DSA effects decay at this temperature and probably do not affect the mobility of dislocations at 500 °C. On the other hand, at 450 °C (Fig. 12) the slip lines look more straight than at 500 °C, as it is expected when the mobility of dislocations are affected by DSA.

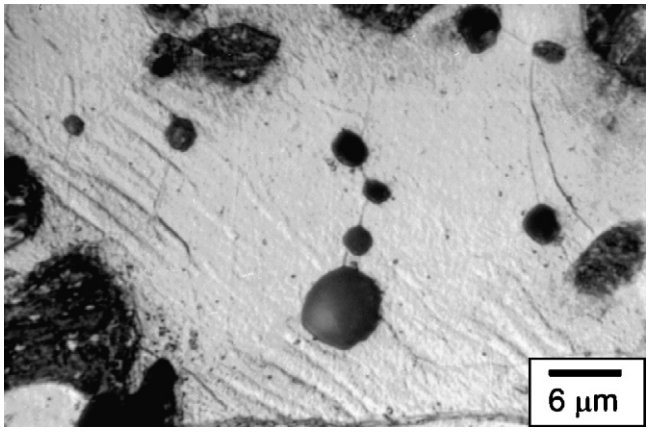

Fig. 13. Optical micrograph of HT samples of AISI 430F cycled over a total strain range $\Delta\varepsilon_t = 0.6\%$ and 500 °C.

At 400 °C and 450 °C, the slip bands are distinctively associated with carbide precipitation. This observation can be explained by considering the diffusion conditions in the slip bands. When the plastic deformation during fatigue concentrates in slip bands, it produces regions of local heating [20]. The heating maintains a super-saturation of carbon during continuous cycling. This appears to provide an explanation of the precipitation reaction at temperatures below the precipitation temperature of 500 °C. During cycling, the precipitates reach a size, note Fig. 12, that is easily observed even with optical microscopy.

At 500 °C, the nucleation of precipitates is not confined to the active slip centers and the matrix exhibits a homogeneous carbide distribution. The synergism between fatigue cycling and temperature allows the large particles to develop and grow at the expense of smaller ones. Fig. 14 is a TEM extraction replica taken from a sample tested at 500 °C. The micrograph illustrates the intense carbide growth experienced in these samples. This observation provides a likely explanation for the pronounced softening that was found at 500 °C. The size of the precipitates increased to the point they no longer served as effective obstacles to dislocation motion, leading to softening.

4. Conclusions

AISI 430F is widely used in structural components and knowledge of its fatigue properties is essential for these applications. We performed low-cycle fatigue tests on this alloy, under total-strain control for temperatures ranging from 20 °C to 500 °C. Our major results follow:

(1) AISI 430F in the HT condition shows pronounced cyclic hardening at 400 °C. This hardening is attributable to DSA. At higher temperatures the initial hardening is followed by a noticeable cyclic softening resulting from carbide growth.
(2) Strain-rate change tests and stress relaxation experiments suggest that DSA takes place in the temperature range between

300 °C and 500 °C. Over this temperature range, carbon solute atoms appear to be responsible for the occurrence of the DSA.

Acknowledgements

This work was supported by 'Agencia Nacional para la Promoción de Ciencia y Técnica' (ANPYCT) and the 'Consejo Nacional de Investigaciones Científicas y Técnicas' (CONICET), from Argentina. The authors are especially grateful to Professor Michael G. Stout for his support and to Mr. Fernando Ugo for assistance with the experiments.

References

[1] K. Tsuzaki, Y. Matsuzaki, T. Maki, I. Tamura, Mater. Sci. Eng. A 142 (1991) 63–70.
[2] M. Weisse, C.K. Wamukwamba, H.J. Christ, H. Mughrabi, Acta Metall. Mater. 41 (1993) 2227–2233.
[3] Y. Estrin, L.P. Kubin, J. Mech. Behav. Mater. 2 (3–4) (1989) 255–292.
[4] L.H. de Almeida, I. Le May, P.R.O. Emygdio, Mater. Charact. 41 (1998) 137–150.
[5] K. Yamaguchi, K. Kanazawa, S. Yoshida, Mater. Sci. Eng. 33 (1978) 175–181.
[6] S. Hong, S. Lee, Int. J. Fatigue 26 (2004) 899–910.
[7] A.F. Armas, O.R. Bettin, I. Alvarez-Armas, G.H. Rubiolo, J. Nuclear Mater. 155–157 (1998) 646–649.
[8] K. Tsuzaki, T. Hori, T. Maki, I. Tamuka, Mater. Sci. Eng. 61 (1983) 247–260.
[9] S.C. Tjong, S.M. Zhu, Metall. Mater. Trans. 28A (1997) 1347–1355.
[10] ASM Handbook, Metallography and Microstructure, vol. 9, ninth ed., ASM International, USA, 1992.
[11] S. Hereñú, I. Alvarez-Armas, A.F. Armas, Scripta Mater. 45 (2001) 739–745.
[12] G.R. Speich, Trans. Metall. Soc. AIME 245 (1969) 2553–2563.
[13] J.R. Davis (Eds.), Stainless Steels, ASM International, Materials Park, OH, 1994.
[14] A.F. Armas, M. Avalos, J. Malarría, I. Alvarez-Armas, C. Petersen, in: K.T. Rie, P.D. Portella (Eds.), Fourth International Conference on Low-cycle Fatigue and Elasto-plastic Behaviour of Materials, Elsevier Science Ltd., 1998, pp. 63–68.
[15] P. Feltham, Philos. Mag. 6 (1961) 259–270.
[16] K.W. Qian, R.E. Reed-Hill, Acta Metall. 31 (1983) 87–94.
[17] C.Y. Jeong, S.W. Nam, J. Ginsztler, Mater. Sci. Eng. A 264 (1999) 188–193.
[18] R. Reed Hill, R. Abbaschian, Physical Metallurgy Principles, third edition, PWS Publishing Company, 1994.
[19] L.H. Van Vlack, Elements of Materials Science and Engineering, Prentice-Hall, 1989.
[20] D.V. Wilson, J.K. Tromans, Acta Metall. 18 (1970) 1197–1208.